JASA EXPRESS LETTERS ARTICLE asa.scitation.org/journal/jel

Analytical solutions for acoustic vortex beam radiation from planar and spherically focused circular pistons

Chirag A. Gokani,[1,2,a] Michael R. Haberman,[1,2] and Mark F. Hamilton[1,2]
[1]Applied Research Laboratories, The University of Texas at Austin, Austin, Texas 78766-9767, USA
[2]Walker Department of Mechanical Engineering, The University of Texas at Austin, Austin, Texas 78712-1063, USA
chiragokani@utexas.edu, haberman@utexas.edu, hamilton@mail.utexas.edu

Abstract: Analytical solutions for acoustic vortex beams radiated by sources with uniform circular amplitude distributions are derived in the paraxial approximation. Evaluation of the Fresnel diffraction integral in the far field of an unfocused source and in the focal plane of a focused source leads to solutions in terms of an infinite series of Bessel functions for orbital numbers $\ell > -2$. These solutions are reduced to closed forms for $0 \leq \ell \leq 4$, which correspond to orbital numbers commonly used in experiments. A scaling law for the vortex ring radius is derived, and its relevance is characterized using ray theory.

[Editor: Régis Marchiano] https://doi.org/10.1121/10.0034739

Received: 19 October 2024 **Accepted:** 5 December 2024 **Published Online:** 24 December 2024

1. Introduction

Acoustic vortex beams possess helical wavefronts characterized by the orbital number ℓ. They were first introduced in acoustics by Hefner and Marston[1,2] and have since been used for particle manipulation,[3–12] underwater communication,[13–19] medical ultrasound,[20–22] and sound diffusion.[23]

Vortex beams can be modeled using Laguerre–Gaussian eigenfunctions,[2] but the fact that an infinite number of terms is needed to match source conditions[24–26] limits their utility. Closed-form analytical solutions are available for Bessel[27–30] and Gaussian[26] vortex beams, but these beams are generated by idealized sources. In practice, acoustic vortex beams are typically radiated from a uniform circular amplitude distribution,[5,9,31–33] often referred to as a circular piston. The goal of the present Letter is to derive analytical solutions in the paraxial approximation for regions of interest in vortex beams radiated by this more commonly employed amplitude distribution.

The Fresnel diffraction integral is used in Sec. 2 to obtain analytical solutions for the far field of an unfocused vortex beam radiated by a source with a uniform circular amplitude distribution. Analytical solutions in the focal plane are obtained in Sec. 3 from the same diffraction integral for a spherically focused source with the same amplitude distribution. In both cases, the analytical solutions are expressed as infinite summations of Bessel functions, which are then reduced to closed forms for orbital numbers $0 \leq \ell \leq 4$. A scaling law for the vortex ring radius is derived in Sec. 4, and its practical relevance is discussed in Sec. 5 by appealing to ray theory. The authors make frequent use of relations developed in their previously published work on vortex beams,[26] referred to below as the companion paper.

2. Unfocused uniform circular vortex source

Solutions of the paraxial equation

$$2ik\frac{\partial q}{\partial z} + \nabla_\perp^2 q = 0 \tag{1}$$

are sought in cylindrical coordinates (r, θ, z) for an unfocused vortex beam having a uniform source pressure p_0 within a circle of radius a,

$$q(r, \theta, 0) = p_0 \,\mathrm{circ}(r/a)\, e^{i\ell\theta}, \tag{2}$$

where $\mathrm{circ}(\alpha) = 1$ for $\alpha \leq 1$ and 0 for $\alpha > 1$. The acoustic pressure with angular frequency ω is $p = qe^{i(kz-\omega t)}$, where $k = \omega/c_0$ is the wavenumber and c_0 is the sound speed. The validity of the paraxial approximation underlying Eq. (1) in the context of vortex beams radiated by unfocused and focused circular pistons has been discussed in Secs. IV and V of the companion paper.[26] The field radiated by a circular piston oscillating in the z direction with velocity u_0 can be

[a]Author to whom correspondence should be addressed.

described in the paraxial approximation by replacing p_0 in Eq. (2) with $\rho_0 c_0 u_0$, where ρ_0 is the ambient density of the fluid.[34]

The Fresnel diffraction integral is an exact solution of Eq. (1) for any source function $q(r,\theta,0)$:

$$q(r,\theta,z) = -\frac{ik}{2\pi z}\int_0^{2\pi}\int_0^{\infty} q(r_0,\theta_0,0)e^{i(k/2z)\left[r^2+r_0^2-2rr_0\cos(\theta_0-\theta)\right]}\, r_0 dr_0 d\theta_0. \tag{3}$$

Combining Eqs. (2) and (3) and applying the relations in Eqs. (8) and (9) of the companion paper[26] yields

$$q(r,\theta,z) = -ikp_0\frac{e^{i(ka^2/2z)r^2/a^2}}{z}e^{i\ell(\theta-\pi/2)}\int_0^a e^{i(ka^2/2z)r_0^2/a^2}J_\ell(krr_0/z)\, r_0 dr_0, \tag{4}$$

where J_n is the Bessel function of the first kind of order n. For $z \gg z_R$, where $z_R = ka^2/2$ is the Rayleigh distance, Eq. (4) reduces to

$$q(r,\theta,z) = -ikp_0\frac{1}{z}e^{i\ell(\theta-\pi/2)}\int_0^a J_\ell(krr_0/z)\, r_0 dr_0\,, \quad z \gg z_R, \tag{5}$$

resulting in the analytical solution

$$q_\ell(r,\theta,z) = -ip_0\frac{z}{kr^2}e^{i\ell(\theta-\pi/2)}F_\ell(kar/z)\,, \quad z \gg z_R, \tag{6}$$

where[35]

$$F_\ell(\xi) = \int_0^\xi J_\ell(t)t\,dt = \xi\,\frac{\Gamma(\ell/2+1)}{\Gamma(\ell/2)}\sum_{k=0}^{\infty}\frac{(\ell+2k+1)\Gamma(\ell/2+k)}{\Gamma(\ell/2+2+k)}J_{\ell+2k+1}(\xi) \tag{7}$$

and Γ is the gamma function. Equation (7), which is restricted to $\ell > -2$, is equivalent to the following closed-form expressions for $0 \le \ell \le 4$:

$$\ell = 0: \quad F_0(\xi) = \xi J_1(\xi), \tag{8a}$$

$$\ell = 1: \quad F_1(\xi) = \frac{\pi}{2}\xi[\mathbf{H}_0(\xi)J_1(\xi) - \mathbf{H}_1(\xi)J_0(\xi)], \tag{8b}$$

$$\ell = 2: \quad F_2(\xi) = 2 - 2J_0(\xi) - \xi J_1(\xi), \tag{8c}$$

$$\ell = 3: \quad F_3(\xi) = \left[\frac{3\pi}{2}\xi\,\mathbf{H}_0(\xi) - 8\right]J_1(\xi) + \left[4\xi - \frac{3\pi}{2}\xi\,\mathbf{H}_1(\xi)\right]J_0(\xi), \tag{8d}$$

$$\ell = 4: \quad F_4(\xi) = 4 - 8J_1(\xi)/\xi - 4J_2(\xi) - \xi J_3(\xi), \tag{8e}$$

where $\mathbf{H}_0$ and $\mathbf{H}_1$ are the zeroth- and first-order Struve functions. In the limiting case $\ell = 0$, Eq. (6) with Eq. (8a) recovers the far-field paraxial pressure radiated by a circular piston,

$$q(r,\theta,z) = -ip_0\frac{ka^2}{2z}\frac{2J_1(kar/z)}{kar/z}\,, \quad z \gg z_R\,, \quad \ell = 0. \tag{9}$$

The validity of Eq. (6) is assessed by comparison with the field calculated using the angular spectrum method,[36]

$$q(x,y,z) = \mathcal{F}_{xy}^{-1}\left\{e^{ik_z z}\mathcal{F}_{xy}[q(x,y,0)]\right\}, \tag{10}$$

where the z component of the wave vector in the paraxial approximation is

$$k_z = k - \frac{k_x^2 + k_y^2}{2k} \tag{11}$$

in order for Eq. (10) to be an exact solution of Eq. (1). The forward and inverse 2D Fourier transforms $\mathcal{F}_{xy}$ and $\mathcal{F}_{xy}^{-1}$ are defined by Eqs. (25) and (26) of the companion paper,[26] with Eq. (2) expressed in Cartesian coordinates as

$$q(x,y,0) = p_0\,\mathrm{circ}\left(\sqrt{x^2+y^2}/a\right)e^{i\ell\arctan(y/x)} \tag{12}$$

for the source function used in Eq. (10), with $\arctan(y/x)$ calculated using the function $\mathrm{atan2}(y,x)$. Equations (10) and (11) combined are equivalent to Eq. (4). In Fig. 1, the validity of the far-field approximation $z \gg z_R$ is assessed by comparing Eqs. (6) and (10) for $0.5 \le z/z_R \le 4$ and $0 \le \ell \le 4$. The comparison reveals that Eq. (6) approximates the exact solution of Eq. (1) reasonably well for $z/z_R \simeq 2$ and that convergence is achieved for $z/z_R \gtrsim 4$.

3. Focused uniform circular vortex source

To describe spherical focusing with a geometric focal length of d in the paraxial approximation, the source condition in Eq. (2) is multiplied by $\exp(-ikr^2/2d)$:

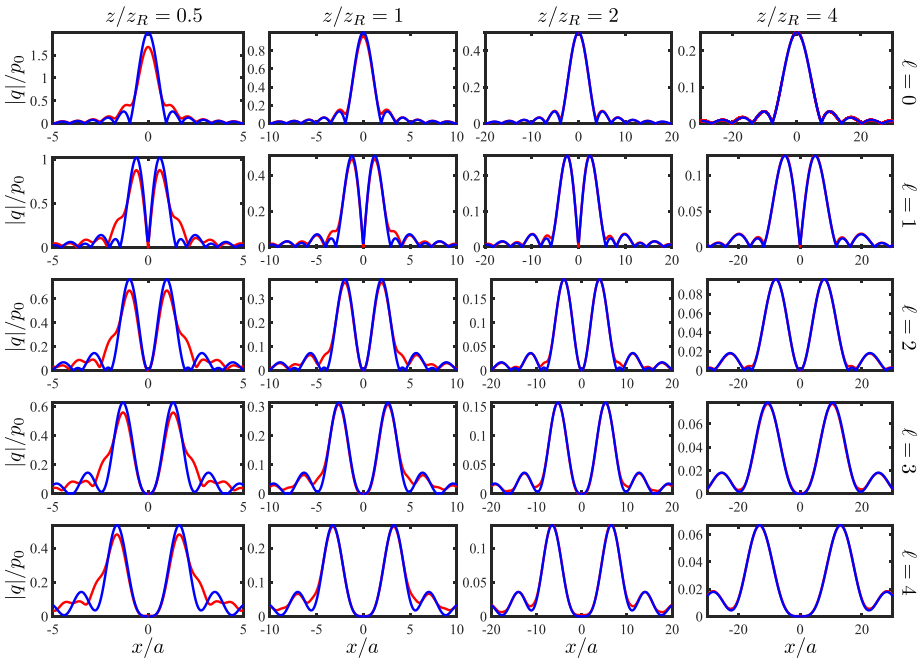

Fig. 1. Comparison of the analytical solution of the paraxial equation in the far field given by Eq. (6) (blue lines) with the numerical solution of the paraxial equation calculated using Eq. (10) (red lines) for the source condition given by Eq. (12) with $0 \le \ell \le 4$ and $z/z_R = 0.5$, 1, 2, and 4.

$$q(r,\theta,0) = p_0\,\mathrm{circ}(r/a)\,e^{-ikr^2/2d}\,e^{i\ell\theta}. \tag{13}$$

Combining Eqs. (3) and (13) and evaluating the integral over θ using Eq. (9) of the companion paper[26] results in

$$q(r,\theta,z) = -ikp_0\,\frac{e^{ikr^2/2z}}{z}\,e^{i\ell(\theta-\pi/2)}\int_0^a e^{i(ka^2/2z)(1-z/d)r_0^2/a^2}J_\ell(krr_0/z)\,r_0 dr_0. \tag{14}$$

The integral reduces to the form of Eq. (7) in the focal plane, $z = d$, resulting in

$$q_\ell(r,\theta,d) = -ip_0\,\frac{d}{kr^2}\,e^{ikr^2/2d}e^{i\ell(\theta-\pi/2)}F_\ell(kar/d), \tag{15}$$

where F_ℓ is given again by Eqs. (8) for $0 \le \ell \le 4$. A solution in the form of Eq. (15) in combination with Eq. (8b) was obtained previously in optics by Sacks *et al.*[37] for $\ell = 1$. In the limiting case $\ell = 0$, Eq. (15) reduces to

$$q(r,\theta,d) = -ip_0\,\frac{ka^2}{2d}\,e^{ikr^2/2d}\,\frac{2J_1(kar/d)}{kar/d}, \quad \ell = 0, \tag{16}$$

recovering the paraxial pressure field in the focal plane of a spherically focused circular piston. Comparison with numerical solutions based on Eqs. (10) and (11), not shown here, reveals that Eq. (15) satisfies Eq. (1), with Eq. (13) expressed in Cartesian coordinates:

$$q(x,y,0) = p_0\,\mathrm{circ}\left(\sqrt{x^2+y^2}/a\right)e^{-ik(x^2+y^2)/2d}\,e^{i\ell\arctan(y/x)}. \tag{17}$$

Limitations on the accuracy of the paraxial approximation for a focused uniform circular piston as the ratio d/a is reduced are assessed as functions of ka and ℓ in the right column of Fig. 5 in the companion paper.[26]

4. Vortex ring radius

The vortex ring radius is a traditional characteristic of a vortex beam in both optics[38,39] and acoustics.[26,30] For unfocused vortex beams, the ring radius is defined as the distance from the z axis to the first local maximum, whereas for focused vortex beams, the definition of ring radius is normally restricted to the focal plane, $z = d$.

The ring radius can be calculated by setting the r derivative of the magnitude of Eqs. (6) and (15) to zero, which is equivalent to solving $d|\xi^{-1}F_\ell(\xi)|/d\xi = 0$, where $\xi = kar/z$ for Eq. (6) and $\xi = kar/d$ for Eq. (15). Using Eq. (7) for F_ℓ leads to the relation[40]

Table 1. Roots ξ_ℓ of Eq. (18) for $1 \le \ell \le 10$.

ℓ	1	2	3	4	5	6	7	8	9	10
ξ_ℓ	2.4516	3.9227	5.2620	6.5356	7.7683	8.9726	10.1559	11.3227	12.4763	13.6191

$$\sum_{k=0}^{\infty} \frac{(\ell+2k+1)\Gamma(\ell/2+k)}{\Gamma(\ell/2+2+k)} \left[\frac{J_{\ell+2k}(\xi) - J_{\ell+2k+2}(\xi)}{2\xi} - \frac{J_{\ell+2k+1}(\xi)}{\xi^2} \right] = 0. \tag{18}$$

The roots ξ_ℓ of Eq. (18) that were found numerically are listed in Table 1 for $1 \le \ell \le 10$. A least-squares fit results in the linear relation

$$\xi_\ell = 1.23\ell + 1.49. \tag{19}$$

The relations $\xi_\ell = kar_\ell/z$ for Eq. (6) and $\xi_\ell = kar_\ell/d$ for Eq. (15) yield

$$r_\ell = \frac{\xi_\ell z}{ka}, \quad z \gg z_R \tag{20}$$

for the ring radius in the far field of an unfocused vortex beam described by Eq. (6) and

$$r_\ell = \frac{\xi_\ell d}{ka}, \quad z = d \tag{21}$$

in the focal plane of a focused vortex beam described by Eq. (15). Practical limitations of Eqs. (20) and (21) are discussed in Sec. 5.

5. Comparisons with ray theory

Equations (20) and (21) accurately predict that the radius of the first local maximum of the magnitudes of Eqs. (6) and (15) is a linear function of ℓ. In practice, however, the position of the global maximum of the field is often of greater interest. Ray theory is used in the companion paper[26] to show that the radial position of the global maximum is a nonlinear function of ℓ for both unfocused and focused vortex beams, which limits the utility of Eqs. (20) and (21).

Since the ray theory developed in the companion paper[26] describes fields that in the immediate vicinity of the source have the form $p \simeq p_0 f(r) e^{i\phi(r,\theta,z)}$, the analysis in that work can be applied to Eq. (2) by setting $\phi = \ell\theta + kz$. Specification of the amplitude distribution $f(r)$ is unnecessary when considering only the geometry of the ray channels and caustics, which is of interest here, not the pressure amplitude predicted by ray theory. For the prescribed phase ϕ, a paraboloidal caustic surface given by Eq. (64) of the companion paper[26] predicts that the radial coordinate of the global maximum is proportional to $\ell^{1/2}$, in contrast with the linear dependence on ℓ predicted by Eq. (20) above for the radius of the first local maximum. The nonlinear dependence on ℓ of the distance from the z axis to the global maximum is demonstrated in Fig. 2, which is generated by overlaying Eqs. (62) and (64) in the companion paper[26] for the ray channels and caustics, respectively, on the amplitude of the paraxial pressure field given by Eqs. (10)–(12).

To apply the analysis in the companion paper[26] to Eq. (13), ϕ is set to $-kr^2/2d + \ell\theta + kz$, for which the global maximum is redistributed over the surface of a spheroidal caustic in the prefocal region given by Eq. (55) of the companion paper, and the distance from the z axis is again proportional to $\ell^{1/2}$. In Fig. 3, the paraxial field corresponding to Eq. (17) for $G = 10$ and 20, where $G = ka^2/2d$ is the focal gain, is calculated and shown together with the ray channels and caustics given by Eqs. (40) and (55) of the companion paper,[26] respectively. Figure 3 shows that while the global

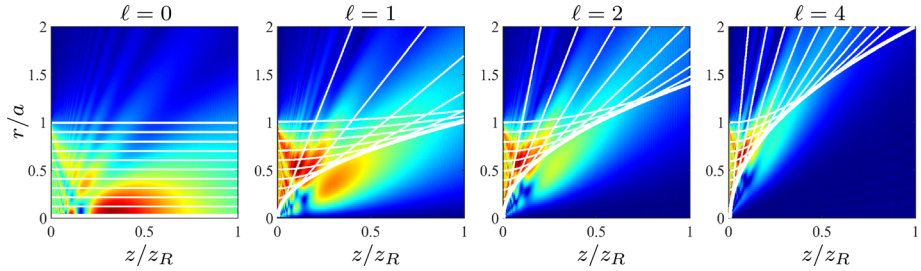

Fig. 2. Overlays of Eqs. (64) and (62) of the companion paper (Ref. 26) for the caustics (thick lines) and annular ray channels (thin lines), respectively, on color plots for the magnitude of the paraxial field obtained from Eqs. (10) and (12) for several values of ℓ. Only ray channels emanating from the circular source occupying the region $r/a \le 1$ are shown. The color plots are normalized such that red corresponds to the maximum pressure amplitude in each subplot and blue corresponds to zero pressure amplitude.

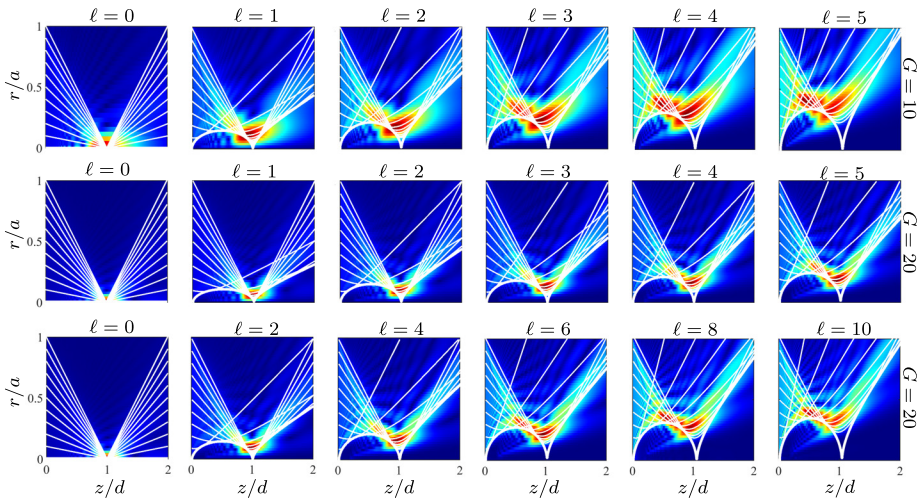

Fig. 3. Overlays of Eqs. (55) and (40) of the companion paper (Ref. 26) for the caustics (thick lines) and annular ray channels (thin lines), respectively, on color plots for the magnitude of the paraxial field obtained from Eqs. (10) and (17) for $G = 10$ (first row) and $G = 20$ (second and third rows) and several values of ℓ. See the caption of Fig. 2 for an explanation of the color map.

maximum conforms to a toroid in the focal plane for low ℓ, it drifts out of the focal plane as ℓ increases, no longer coinciding with the vortex ring radius provided by Eq. (21).

The paraxial solutions for $f(r) = \mathrm{circ}(r/a)$ in Figs. 2 and 3 do not conform as well to the caustics as do the paraxial solutions for the Gaussian amplitude distribution $f(r) = e^{-r^2/a^2}$ in Figs. 8 and 9 of the companion paper.[26] The discrepancies are due to the discontinuity of $f(r) = \mathrm{circ}(r/a)$ at $r = a$, which makes the effects of diffraction substantially more prominent in the present work than in the companion paper.[26] Despite the complexity of the field, the diffraction patterns in Figs. 2 and 3 are coincident with the features of the ray channels, and the caustics are reasonable demarcations of borders of the global maxima and shadow zones for $\ell > 0$. As G is increased in Fig. 3, the diffraction and ray features align better because increasing ka tends toward the infinite frequency limit that underlies ray theory. Although the orbital numbers and focal gains are different for each plot in the first and third rows, the caustics and ray channels are identical in those two rows because they are invariant for constant ℓ/k (see Ref. 26), corresponding to constant ℓ/G in Fig. 3.

It is noted that for the raised cosine source function mentioned two paragraphs above Eq. (62) in the companion paper[26] as a practical approximation of an infinitely wide Gaussian source function, the raised cosine should have an upper limit of $2a$ instead of a.

6. Conclusion

The Fresnel diffraction integral was used to derive analytical solutions in the paraxial approximation for acoustic vortex beams radiated by uniform circular amplitude distributions. The solutions are valid in the far field of an unfocused source and in the focal plane of a focused source. Diffraction theory predicts that the radius of the vortex ring in these regions increases linearly with ℓ, while ray theory predicts that the distance from the beam axis to the global maximum in the field increases nonlinearly with ℓ. The analytical solutions may prove useful for investigating various features of vortex beams radiated by circular pistons.

Acknowledgments

C.A.G. was supported by the Applied Research Laboratories Chester M. McKinney Graduate Fellowship in Acoustics.

Author Declarations

Conflict of Interest

The authors have no conflicts to disclose.

Data Availability

The data that support the findings of this study are available within the article.

References

[1]B. T. Hefner and P. L. Marston, "Acoustical helicoidal waves and Laguerre-Gaussian beams: Applications to scattering and to angular momentum transport," J. Acoust. Soc. Am. **103**, 2971 (1998).

[2]B. T. Hefner and P. L. Marston, "An acoustical helicoidal wave transducer with applications for the alignment of ultrasonic and underwater systems," J. Acoust. Soc. Am. **106**, 3313–3316 (1999).
[3]S. T. Kang and C. K. Yeh, "Potential-well model in acoustic tweezers," IEEE Trans. Ultrason. Ferroelectr. Freq. Control **57**, 1451–1459 (2010).
[4]L. Zhang and P. L. Marston, "Angular momentum flux of nonparaxial acoustic vortex beams and torques on axisymmetric objects," Phys. Rev. E **84**, 065601 (2011).
[5]A. Anhäuser, R. Wunenburger, and E. Brasselet, "Acoustic rotational manipulation using orbital angular momentum transfer," Phys. Rev. Lett. **109**, 034301 (2012).
[6]D. Baresch, J.-L. Thomas, and R. Marchiano, "Spherical vortex beams of high radial degree for enhanced single-beam tweezers," J. Appl. Phys. **113**, 184901 (2013).
[7]R. Wunenburger, J. I. V. Lozano, and E. Brasselet, "Acoustic orbital angular momentum transfer to matter by chiral scattering," New J. Phys. **17**, 103022 (2015).
[8]Z. Hong, J. Zhang, and B. W. Drinkwater, "Observation of orbital angular momentum transfer from Bessel-shaped acoustic vortices to diphasic liquid-microparticle mixtures," Phys. Rev. Lett. **114**, 214301 (2015).
[9]T. Wang, M. Ke, W. Li, Q. Yang, C. Qiu, and Z. Liu, "Particle manipulation with acoustic vortex beam induced by a brass plate with spiral shape structure," Appl. Phys. Lett. **109**, 123506 (2016).
[10]M. Baudoin, J.-C. Gerbedoen, A. Riaud, O. B. Matar, N. Smagin, and J.-L. Thomas, "Folding a focalized acoustical vortex on a flat holographic transducer: Miniaturized selective acoustical tweezers," Sci. Adv. **5**, eaav1967 (2019).
[11]Z. Gong and M. Baudoin, "Particle assembly with synchronized acoustic tweezers," Phys. Rev. Appl. **12**, 024045 (2019).
[12]A. Marzo and B. W. Drinkwater, "Holographic acoustic tweezers," Proc. Natl. Acad. Sci. U.S.A. **116**, 84–89 (2019).
[13]T. M. Marston and P. L. Marston, "Modulated helicity for acoustic communications and helicity-selective acoustic receivers," J. Acoust. Soc. Am. **127**, 1856 (2010).
[14]V. Bollen, D. J. Zartman, T. M. Marston, and P. L. Marston, "Measured scattering of a first-order vortex beam by a sphere: Cross-helicity and helicity-neutral near-forward scattering and helicity modulation," Proc. Mtgs. Acoust. **19**, 070075 (2013).
[15]C. Shi, M. Dubois, Y. Wang, and X. Zhang, "High-speed acoustic communication by multiplexing orbital angular momentum," Proc. Natl. Acad. Sci. U.S.A. **114**, 7250–7253 (2017).
[16]X. Jiang, B. Liang, J.-C. Cheng, and C.-W. Qiu, "Twisted acoustics: Metasurface-enabled multiplexing and demultiplexing," Adv. Mater. **30**, 1800257 (2018).
[17]X. Jiang, C. Shi, Y. Wang, J. Smalley, J. Cheng, and X. Zhang, "Nonresonant metasurface for fast decoding in acoustic communications," Phys. Rev. Appl. **13**, 014014 (2020).
[18]Z. Sun, Y. Shi, X. Sun, H. Jia, Z. Jin, K. Deng, and J. Yang, "Underwater acoustic multiplexing communication by pentamode metasurface," J. Phys. D: Appl. Phys. **54**, 205303 (2021).
[19]M. E. Kelly and C. Shi, "Design and simulation of acoustic vortex wave arrays for long-range underwater communication," JASA Express Lett. **3**, 076001 (2023).
[20]A. Ozcelik, J. Rufo, F. Guo, Y. Gu, P. Li, J. Lata, and T. J. Huang, "Acoustic tweezers for the life sciences," Nat. Methods **15**, 1021–1028 (2018).
[21]S. Jiménez-Gambín, N. Jiménez, and F. Camarena, "Transcranial focusing of ultrasonic vortices by acoustic holograms," Phys. Rev. Appl. **14**, 054070 (2020).
[22]S. Guo, Z. Ya, P. Wu, L. Zhang, and M. Wan, "Enhanced sonothrombolysis induced by high-intensity focused acoustic vortex," Ultrasound Med. Biol. **48**, 1907–1917 (2022).
[23]N. Jiménez, J. P. Groby, and V. Romero-García, "Spiral sound-diffusing metasurfaces based on holographic vortices," Sci. Rep. **11**, 10217 (2021).
[24]R. Marchiano and J.-L. Thomas, "Synthesis and analysis of linear and nonlinear acoustical vortices," Phys. Rev. E **71**, 066616 (2005).
[25]X. Pan, J. Wu, Z. Li, C. Zhang, C. Deng, Z. Zhang, H. Wen, Q. Gao, J. Yang, Z. Yi, M. Yu, L. Liu, F. Chi, and P. Bai, "Laguerre-Gaussian mode purity of Gaussian vortex beams," Optik **230**, 166320 (2021).
[26]C. A. Gokani, M. R. Haberman, and M. F. Hamilton, "Paraxial and ray approximations of acoustic vortex beams," J. Acoust. Soc. Am. **155**, 2707–2723 (2024).
[27]P. L. Marston, "Scattering of a Bessel beam by a sphere: II. Helicoidal case and spherical shell example," J. Acoust. Soc. Am. **124**, 2905–2910 (2008).
[28]P. L. Marston, "Radiation force of a helicoidal Bessel beam on a sphere," J. Acoust. Soc. Am. **125**, 3539–3547 (2009).
[29]L. Zhang and P. L. Marston, "Geometrical interpretation of negative radiation forces of acoustical Bessel beams on spheres," Phys. Rev. E **84**, 035601 (2011).
[30]N. Jiménez, R. Picó, V. Sánchez-Morcillo, V. Romero-García, L. M. García-Raffi, and K. Staliunas, "Formation of high-order acoustic Bessel beams by spiral diffraction gratings," Phys. Rev. E **94**, 053004 (2016).
[31]D. Baresch, J. L. Thomas, and R. Marchiano, "Observation of a single-beam gradient force acoustical trap for elastic particles: Acoustical tweezers," Phys. Rev. Lett. **116**, 024301 (2016).
[32]M. E. Terzi, S. A. Tsysar, P. V. Yuldashev, M. M. Karzova, and O. A. Sapozhnikov, "Generation of a vortex ultrasonic beam with a phase plate with an angular dependence of the thickness," Moscow Univ. Phys. Bull. **72**, 61–67 (2017).
[33]J. Li, A. Crivoi, X. Peng, L. Shen, Y. Pu, Z. Fan, and S. A. Cummer, "Three dimensional acoustic tweezers with vortex streaming," Commun. Phys. **4**, 113 (2021).
[34]E. A. Zabolotskaya and R. V. Khokhlov, "Quasi-plane waves in the nonlinear acoustics of confined beams," Sov. Phys. Acoust. **15**, 35–40 (1969).
[35]M. Abramowitz and I. A. Stegun, *Handbook of Mathematical Functions*, 4th ed. (Dover Publications, New York, 1972), Item 11.1.1.
[36]E. G. Williams, *Fourier Acoustics* (Academic Press, San Diego, 1999), Sec. 2.9.

[37]Z. S. Sacks, D. Rozas, and G. A. Swartzlander, Jr., "Holographic formation of optical-vortex filaments," J. Opt. Soc. Am. B **15**, 2226–2234 (1998).
[38]M. Padgett and L. Allen, "The Poynting vector in Laguerre-Gaussian laser modes," Opt. Commun. **121**, 36–40 (1995).
[39]J. E. Curtis and D. G. Grier, "Structure of optical vortices," Phys. Rev. Lett. **90**, 485–487 (2003).
[40]I. S. Gradshteyn and I. M. Ryzhik, *Table of Integrals, Series, and Products*, 4th ed. (Academic Press, New York, 1980), Item 8.471-2.